AGU PUBLICATIONS

Global Biogeochemical Cycles

RESEARCH ARTICLE
10.1002/2014GB004939

Key Points:
- We track the history of Hg pollution since the Spanish colonial period
- The first study with both 3-D oceanic and atmospheric transport for Hg
- Constrained lake sediment observations and oceanic profiles of Hg

Supporting Information:
- Readme
- Figures S1 and S2 and Table S1

Correspondence to:
L. Jaeglé,
jaegle@atmos.washington.edu

Citation:
Zhang, Y., L. Jaeglé, L. A. Thompson, and D. G. Streets (2014), Six centuries of changing oceanic mercury, *Global Biogeochem. Cycles*, *28*, doi:10.1002/2014GB004939.

Received 19 JUL 2014
Accepted 12 OCT 2014
Accepted article online 15 OCT 2014

Six centuries of changing oceanic mercury

Yanxu Zhang[1,2], Lyatt Jaeglé[1], LuAnne Thompson[3], and David G. Streets[4]

[1]Department of Atmospheric Sciences, University of Washington, Seattle, Washington, USA, [2]Now at School of Engineering and Applied Sciences, Harvard University, Cambridge, Massachusetts, USA, [3]School of Oceanography, University of Washington, Seattle, Washington, USA, [4]Decision and Information Sciences Division, Argonne National Laboratory, Argonne, Illinois, USA

Abstract Mercury (Hg) is a global and persistent contaminant, affecting human health primarily via marine fish consumption. Large anthropogenic releases of Hg to the atmosphere by mining and coal combustion have resulted in a significant perturbation to the biogeochemical cycling of Hg. The magnitude of this perturbation and the relative roles of the ocean and land as sinks for anthropogenic Hg remain unclear. Here we use a 3-D global ocean biogeochemical model to show that surface ocean Hg concentrations have increased fourfold over the last 600 years. We find that anthropogenic Hg enters the ocean's interior predominantly by absorption onto sinking organic matter particulates, which decompose and release Hg at a depth of 500–800 m, implying that the human perturbation is largest in subsurface waters of biologically productive regions. Our model simulation predicts that over the last six centuries half of emitted anthropogenic Hg has accumulated in the oceans and marine sediments.

1. Introduction

Anthropogenic emissions of mercury (Hg) to the environment date back to the early history of human civilization. Prior to 1850, atmospheric emissions were primarily from Hg mining and use of Hg in amalgam extraction of gold and silver ores [*Lacerda*, 1997; *Nriagu*, 1993; *Streets et al.*, 2011]. Since the industrial revolution, coal combustion has become the dominant source of Hg, accounting for nearly half of present-day anthropogenic Hg emissions [*Pacyna et al.*, 2010]. Once in the atmosphere, Hg is transported globally until it deposits onto the Earth's surface, where it bioaccumulates in aquatic food chains as highly toxic methylmercury [*Fitzgerald et al.*, 2007; *Morel et al.*, 1998]. Natural archives of atmospheric deposition from lake sediments, peat bogs, and ice cores suggest that the current Hg deposition flux to land is 2–5 times higher than in 1850 [*Fitzgerald et al.*, 2005]. Available records extending back several thousand years show even larger increases [*Cooke et al.*, 2009; *Elbaz-Poulichet et al.*, 2011].

Little is known about how human perturbation has affected the marine biochemical cycling of Hg, what fraction of anthropogenic Hg has accumulated in the oceans, or what areas of the oceans are most affected. These uncertainties severely limit our ability to understand the past and predict the future Hg concentrations in the oceans and their impact on Hg content in marine fish. In particular, the response of marine Hg to ongoing and planned reductions in anthropogenic emissions will be highly dependent on contributions from historical sources. Oceanic measurements of Hg profiles remain very sparse and display large interlaboratory variability, making spatial and temporal trends in marine Hg concentrations difficult to assess observationally [*Fitzgerald et al.*, 2007; *Mason et al.*, 2012]. Modeling studies predict factors of 1.25 to 3 increase in surface ocean Hg concentrations since 1850 [*Mason et al.*, 1994; *Lamborg et al.*, 2002; *Mason and Sheu*, 2002; *Sunderland and Mason*, 2007; *Selin et al.*, 2008] and factors of 3.6–6 increase when compared with natural conditions and taking into account pre-1850 anthropogenic emissions [*Streets et al.*, 2011; *Amos et al.*, 2013]. Large disagreement is found among estimates of the mass of anthropogenic Hg residing in the ocean, ranging from 120 Mmol [1 Mmol = 10^6 mol] to 1100 Mmol [*Streets et al.*, 2011; *Mason et al.*, 1994; *Lamborg et al.*, 2002; *Mason and Sheu*, 2002; *Sunderland and Mason*, 2007; *Selin et al.*, 2008; *Amos et al.*, 2013]. These variations reflect uncertainties in emissions of anthropogenic Hg over the last centuries, as well as treatment of oceanic transport in a simplified manner. Indeed, current global ocean Hg models represent the ocean as 1–3 boxes in the vertical and/or neglect horizontal transport [e.g., *Sunderland and Mason*, 2007; *Amos et al.*, 2013]. These simplifications are problematic as the intermediate and deep oceans are not well mixed on the 200–600 year timescale of the anthropogenic Hg perturbation [*Siegenthaler and Oeschger*, 1978; *Joos et al.*, 1996; *Strode et al.*, 2010].

We examine the distribution and evolution of anthropogenic Hg in the ocean using a global 3-D ocean tracer model coupled with global 3-D atmosphere-land model [*Zhang et al.*, 2014; *Holmes et al.*, 2010]. This framework, with realistic treatment of oceanic and atmospheric transport, allows us to place new constraints on the human perturbation to the Hg cycle via direct comparisons to (1) lake sediment observations of the temporal and spatial changes in deposition to land, and (2) oceanic profiles of Hg in different ocean basins representing the cumulative anthropogenic input. In our model, Hg enters the ocean from atmospheric deposition and riverine effluents. Hg biochemistry in the ocean tracer model includes air-sea exchange, biological, and photochemical Hg redox chemistry, as well as reversible sorption onto organic particles and coupling to the biological pump (see section 2). As part of the biological pump, the Hg absorbed on organic particles sinks to the intermediate and deep ocean waters, where bacterial remineralization leads to the release of Hg [*Mason and Fitzgerald,* 1993; *Mason et al.*, 1998].

2. Methods

We couple an offline ocean tracer model (OFFTRAC-Hg) with an atmospheric chemical transport model (GEOS-Chem) to simulate the Hg cycle in this study. The details of these models are elaborated below:

2.1. OFFTRAC-Hg Model

OFFTRAC model is an offline advection/diffusion ocean tracer model. It uses archived monthly averaged transport fields from the Hallberg Isopycnal Model (HIM) [*Hallberg and Rhines*, 1996; *Ladd and Thompson*, 2001]. The world's oceans are resolved on a nominal 1° latitude by 1° longitude with 1/3° latitude resolution in the equatorial ocean. The model has 49 isopycnal layers containing two layers of Kraus-Turner-type mixed layer and two buffer layers. The HIM model is run for 650 years with climatological forcing at the surface by prescribed atmospheric boundary conditions (CORE-II) [*Large and Yeager*, 2009] and then integrated further using interannanually varying winds, air temperatures, and humidity from the National Centers for Environmental Prediction reanalysis between 1950 and 2006 [*Kalnay et al.*, 1996]. The Hg modeling capability in the OFFTRAC model was developed and described in *Zhang et al.* [2014]. Briefly, the OFFTRAC-Hg model simulates three Hg tracers: dissolved elemental mercury (Hg^0_{aq}), dissolved oxidized mercury (Hg^{II}_{aq}), and mercury bound to particulate matter (Hg^P_{aq}). We assume that Hg input to the ocean is via atmospheric deposition and riverine effluent input (both in the form of Hg^{II}_{aq}). We simulate the air-sea exchange of Hg^0_{aq} with atmosphere, and the redox reactions between Hg^0_{aq} and Hg^{II}_{aq} in the ocean water. Hg^{II}_{aq} and Hg^P_{aq} are assumed to be in instantaneous partitioning equilibrium, and the fraction of Hg^P_{aq} relative to Hg^{II}_{aq} is proportional to the local levels of particulate organic carbon (POC). We also include the sink of Hg^P_{aq} along with sinking POC as part of the biological pump in the OFFTRAC model. The POC sinking flux is derived from satellite-retrieved net primary production following *Dunne et al.* [2005].

2.2. GEOS-Chem Model

The GEOS-Chem model is driven by assimilated meteorological observations from the NASA Goddard Earth Observing System (GEOS) (www.geos-chem.org). In this paper, we use version v9-01-02. The meteorological fields have a horizontal resolution of 4° latitude by 5° longitude and 47 vertical levels. In our simulation, we use GEOS-5 repeating meteorological fields for the year 2006. The GEOS-Chem atmospheric Hg simulation was described in *Selin et al.* [2007], with more recent updates in *Holmes et al.* [2010], *Amos et al.* [2012], and *Zhang et al.* [2012]. This model simulates two atmospheric Hg tracers: elemental mercury (Hg^0) and divalent mercury (Hg^{II}). The Hg chemistry in this model includes the oxidation of Hg^0 by Br atom and the in-cloud reduction of Hg^{II}. The model contains a surface soil module with prescribed soil Hg concentration distribution. The soil Hg^0 reemission is dynamically simulated according to meteorological conditions [*Selin et al.*, 2007].

2.3. Model Coupling

Atmospheric transport within GEOS-Chem is calculated with a 60 min time step, while in OFFTRAC we use a daily time step for the mixed layer and a monthly time step for the rest of the ocean. Coupling between the OFFTRAC and GEOS-Chem simulations occurs once a month. GEOS-Chem provides to OFFTRAC three variables: atmospheric Hg^0 concentrations, Hg^{II} deposition fluxes, and riverine input, while OFFTRAC provides to GEOS-Chem the net Hg^0 evasion flux. These variables are all archived on a monthly basis. Riverine flux of Hg from land to ocean is also calculated from the soil Hg concentration distribution around

Table 1. Detailed Information for the Source of Oceanic Observations Shown in Figure 4

Ocean Basin	Symbol[a]	Cruise Name	Latitude/Longitude Range	Time	References
Subarctic Atlantic	●	IOC 1993	47°N–68°N, 60°W–0°W	Aug 1993	*Mason et al.* [1998]
Midlatitude North Atlantic	●	BATS	31°N, 64°W	Mar 2000	*Mason et al.* [2001]
	▲	BATS	31°N, 64°W	Jun 2008	*Lamborg et al.* [2012]
	▼	GEOTRACES GA03	20°N–23°N, 26°W–39°W	Nov to Dec 2011	*Bowman et al.* [2014]
Equatorial Atlantic	●	Knorr	0.6°S, 20°W	Jun 1996	*Mason and Sullivan* [1999]
	▲	GEOTRACES GA02	13°S–0°S, 28°W–33°W	Mar 2011	*Bowman et al.* [2012]
South Atlantic	●	Knorr	33°S, 40°W	Jun 1996	*Mason and Sullivan* [1999]
	▲	Knorr	17°S, 25°W	Jun 1996	*Mason and Sullivan* [1999]
	▼	GEOTRACES GA02	23°S–49°S, 33°W–49°W	Mar 2011	*Bowman et al.* [2012]
Southern Ocean	●	SR3 CASO-GEOTRACES	44°S–57°S, 140°E–147°E	Mar to Apr 2008	*Cossa et al.* [2011]
	▲		57°S–66°S, 140°E–147°E		
Equatorial Pacific		RITS	20°S–10°N, 170°E–70°W	Jan to Feb 1990	*Mason and Fitzgerald* [1993]
North Pacific		CLIVAR-P16N	20°N–60°N, 152°W	Mar 2006	*Sunderland et al.* [2009]
North Pacific (20°N–35°N)	●	SAFe	30°N, 140°W	May 2009	*Hammerschmidt and Bowman* [2012]
	▲	IOC 2002	23°N, 158°E	May to Jun 2002	*Laurier et al.* [2004]
North Pacific (35°N–60°N)	●	IOC 2002	44°N, 155°E	May to Jun 2002	*Laurier et al.* [2004]
	▲	VERTEX	48°N, 148°W	Jul to Aug 1987	*Laurier et al.* [2004]

[a]The symbols correspond to individual profiles shown in Figures 4c–4i.

river mouths and the climatological monthly mean fresh water discharge from continents [*Dai and Trenberth*, 2002]. We used the soil Hg concentration predicted by *Streets et al.* [2011] with a global average of 16 ppb under natural conditions.

2.4. Simulation for 1450–2008

We first run our coupled model system for preanthropogenic conditions [*Zhang et al.*, 2014]. Once the ocean has reached steady state (after ~10,000 years), we conduct a time-dependent simulation with increasing anthropogenic emissions using the historical anthropogenic Hg emission inventory developed by *Streets et al.* [2011] starting from year 1450 until 2008. This inventory provides global total anthropogenic Hg emissions during 1450–1850, and detailed decadal Hg emissions for 1850–2008 by region (North America, South America, Europe, Former USSR, Africa and Mideast, Asia, and Oceania), source type (silver mining, artisanal gold mining, large-scale gold mining, waste incineration, coal combustion, other metal production, etc.), and speciation (Hg^0 and Hg^{II}). On a subregional basis, we allocate gold/silver/mercury mining based on historical mining locations [*Lacerda*, 1997] and other anthropogenic emissions are distributed following the present-day geographical distribution within each region [*Pacyna et al.*, 2010]. In a sensitivity simulation, we decrease the Hg emissions from mining in the Streets inventory by a factor of 3 prior to 1920 [*Guerrero*, 2012]. This leads to a simulation of deposition to land that is more consistent with historical archives from lake core sediments (see section 3.1).

2.5. Observational Data Sets

We compiled 120 lake sediment profiles and 88 oceanic total Hg concentration profiles reported in the literature (see Table 1 and Table S1 in the supporting information for a full list of references). For the lake sediments, we normalized the Hg accumulation flux rates to the levels in the earliest part of the record (observations in 1800 for most of the sites). Multiple profiles sampled at nearby locations are combined, and the mean value and standard deviation are shown.

3. Results and Discussion

3.1. Time Evolution of Hg Emissions, Deposition, and Ocean Concentrations

Starting from a preanthropogenic ocean and atmosphere [*Zhang et al.*, 2014], we performed a time-dependent coupled ocean-atmosphere-land Hg simulation with anthropogenic emissions from year 1450 to 2008 [*Streets et al.*, 2011]. Since 1950, the increase in Hg emissions has been dominated by unintentional release of the toxic metal during coal combustion (Figure 1a). Anthropogenic emissions of Hg in 1450–1850 are due to silver mining in South and Central America, followed by extensive Hg mining and its use in gold and

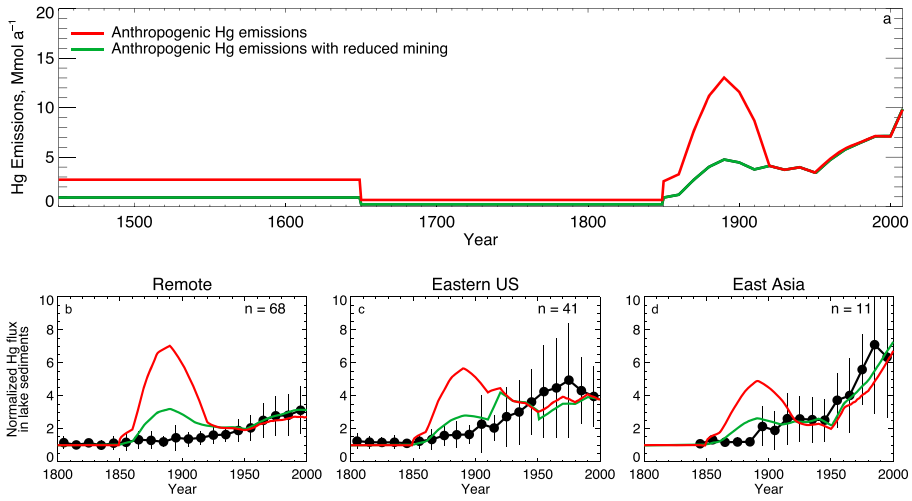

Figure 1. Historical trends in anthropogenic Hg emissions and Hg accumulation flux to lake sediments. (a) Global anthropogenic Hg emissions between 1450 and 2008. The emission inventory from Streets et al. (3) is shown in red, while the emission inventory with mining emissions reduced by a factor of 3 is shown in green. Mean historical Hg flux inferred from sediment cores in (b) 68 remote lakes, (c) 41 lakes in the eastern U.S., and (d) 11 lakes in East Asia. All the fluxes are normalized to 1800–1850 levels. Observations (black filled circles with vertical line showing 1σ) are compared against model results (red and green lines correspond to the original and reduced mining inventories, respectively).

silver extraction in North America between 1850 and 1920. We have compiled historical Hg deposition records in 120 lake sediment cores (see section 2) and found that the *Streets et al.* [2011] emission inventory resulted in significant overestimates of Hg deposition from 1850 to 1920 (Figures 1b–1d). Although the amount of Hg used in precious metal extraction is reasonably well known [*Streets et al.*, 2011; *Nriagu,* 1993], there is a debate as to what fraction volatilized to the atmosphere [*Strode et al*., 2009; *Engstrom et al.*, 2014]. *Streets et al.* [2011] assumed that 52% of the Hg used in historical Au/Ag mining was volatized to the atmosphere, consistent with previous studies [*Nriagu*, 1993; *Lacerda*, 1997]. The work of *Guerrero* [2012] suggests that 66–93% of the Hg used in Au/Ag mining formed solid calomel (Hg_2Cl_2), which was trapped in Au/Ag mining waste and washed downstream or buried in landfills. Thus, only 34–7% of the Hg used might have volatilized to the atmosphere. We find that a simulation with mining releases to the atmosphere decreased by a factor of 3 prior to 1920 is more consistent with these environmental archives (Figures 1b–1d). Our simulation thus assumes that 17% of the Hg used in mining was released to the atmosphere, within the range found by *Guerrero* [2012]. The resulting total cumulative anthropogenic Hg emissions are reduced from 1750 Mmol to 950 Mmol. In the rest of the analysis presented here we use the results from this simulation with reduced mining emissions.

The 7 month atmospheric lifetime of Hg [*Holmes et al.*, 2010; *Zhang et al.*, 2014] allows the modeled Hg in the atmosphere to closely track changing anthropogenic Hg emissions (Figure 2a). Our simulation predicts that atmospheric Hg concentrations have increased by a factor of 5.5 over the last 600 years, reaching a global mean value of 1.2 ng/m^3. This modeled present-day Hg concentration is consistent with observed values of 1.0–1.5 ng/m^3 [*Ebinghaus et al.*, 2009; *Sprovieri et al.*, 2010] (see Figures S1 and S2 in the supporting information). Increasing atmospheric Hg levels have resulted in a factor of 4.8 increase in deposition to the ocean and 7.5 increase in deposition to land. Overall the model reproduces the evolution of the observed enhancement in deposition as recorded in lake sediment cores (Figures 1b–1d). Remote lakes have an average enrichment factor (defined as the ratio of Hg accumulation flux for the present-day relative to 1800) of 3, consistent with previous studies [e.g., *Fitzgerald et al.*, 2005]. Both observations and model display larger increases in Hg deposition fluxes in the eastern U.S. (factor of 4) and East Asia (factor of 6), reflecting the stronger influence of regional Hg emissions in these industrialized areas.

About 90% of the Hg input to the surface ocean is via atmospheric deposition [*Strode et al.*, 2007; *Mason et al.,* 2012], while the majority of its loss is via air-sea exchange, leading to a 7 month lifetime for Hg in the

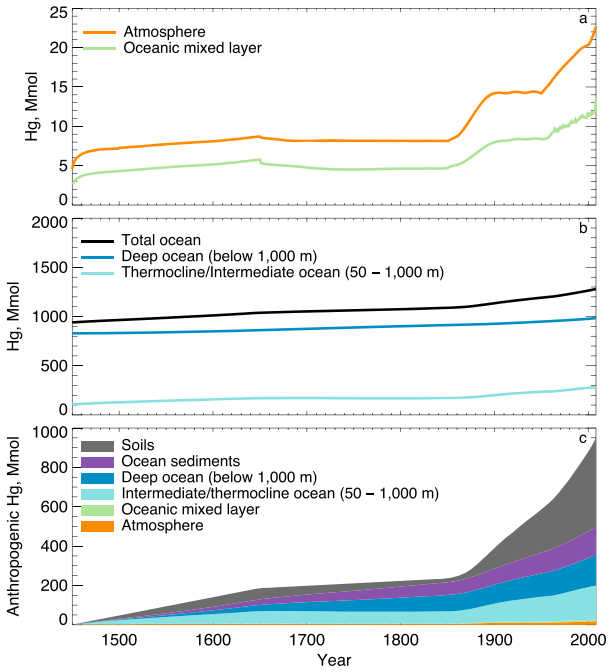

Figure 2. Modeled time evolution of Hg in the atmosphere, ocean, and land reservoirs. Evolution of Hg (in units of Mmol) in the (a and b) atmosphere and ocean reservoirs. The ocean mixed layer represents the top 50 m of the ocean; the thermocline and intermediate oceans are for depths ranging from 50 m to 1000 m, and the deep ocean is below 1000 m. (c) Storage of anthropogenic Hg in environmental reservoirs.

ocean mixed layer (top most 50 m) [*Zhang et al.*, 2014]. We find that Hg in the ocean mixed layer increases by a factor of 4.4, quickly responding to the increasing atmospheric Hg deposition (Figure 2a). We calculate a mean present-day surface ocean Hg concentration of 0.72 pM, within the range of observed values (0.1 pM–7 pM) with a median of 1 pM [*Fitzgerald et al.*, 2007; *Soerensen et al.*, 2010] (see Figures S1 and S2 in the supporting information). The modeled mean residence time of Hg in the thermocline/intermediate ocean (~50–1000 m) is 120 years and for the deep ocean (depths greater than 1000 m) it is 2000 years [*Zhang et al.*, 2014]. Thus, the temporal trends of Hg in these reservoirs are much slower and smoother than in the mixed layer (Figure 2b). The mass of Hg in the thermocline/intermediate ocean increases by 50%, while in the deep ocean it increases by 20%.

Our model predicts that the Hg mass in the global ocean has increased from 960 Mmol to 1290 Mmol (330 Mmol increase). Within the ocean, we find that 45% of the anthropogenic Hg is in the deep ocean, 52% is in the thermocline/intermediate ocean, and 2.8% in the mixed layer (Figure 2c). About 67% of the increase of oceanic Hg mass (220 Mmol) occurred before 1920 owing to mining activities. The coal surge since 1920 contributes to the remaining anthropogenic Hg in the ocean. Our results for the ocean mixed layer are comparable to two box model studies of *Streets et al.* [2011] and *Amos et al.* [2013], which reported factors of 3.6–5.9 increase (compared to 4.4 in our study). However, these studies report larger increases in the thermocline/intermediate ocean (factors of 2.7–5.3, 560–570 Mmol, compared to a factor of 1.5 and 170 Mmol in our study) and in the deep ocean (factors of 1.5–2.1, 500–520 Mmol, compared to a factor of 1.2 and 140 Mmol in our study). These differences are due to an overestimate of the vertical mixing of anthropogenic Hg in the box model studies combined with higher assumed mining emissions. Our results are similar to the 290 ± 80 Mmol anthropogenic Hg burden in the oceans reported by *Lamborg et al.* [2014a] using a method combining Hg observations with anthropogenic CO_2 as a proxy. *Lamborg et al.* [2014a] calculates that 6% of anthropogenic Hg resides in the surface ocean, 59% in the thermocline/intermediate, and 35% in the deep ocean. Our vertical distribution of anthropogenic Hg within the ocean is comparable (3% surface, 52% thermocline/intermediate, and 45% deep ocean), but we find significantly more anthropogenic Hg in the deep ocean than *Lamborg et al.* [2014a].

Overall, the emission inventory adopted in this study leads to a cumulative anthropogenic Hg release of 950 Mmol over the last 600 years, with 650 Mmol from metal mining, 200 Mmol from coal combustion, and the remaining 100 Mmol from other industrial sources. Our model predicts that today, 2% (18 Mmol) of the cumulative anthropogenic Hg is in the atmosphere, 48% (460 Mmol) is in soils, 35% (330 Mmol) is in the ocean, and 15% (140 Mmol) is in ocean sediments (Figure 2c).

3.2. Distribution of Present-Day Oceanic Hg

Examination of both horizontal and vertical distributions of Hg in the ocean reveals the control of atmospheric deposition processes, oceanic advective pathways, and the oceanic biological pump. The mixed layer Hg concentrations (Figure 3a) are enhanced in regions with high atmospheric wet deposition, in particular along the midlatitude storm tracks, high riverine input along coasts, and regions of strong

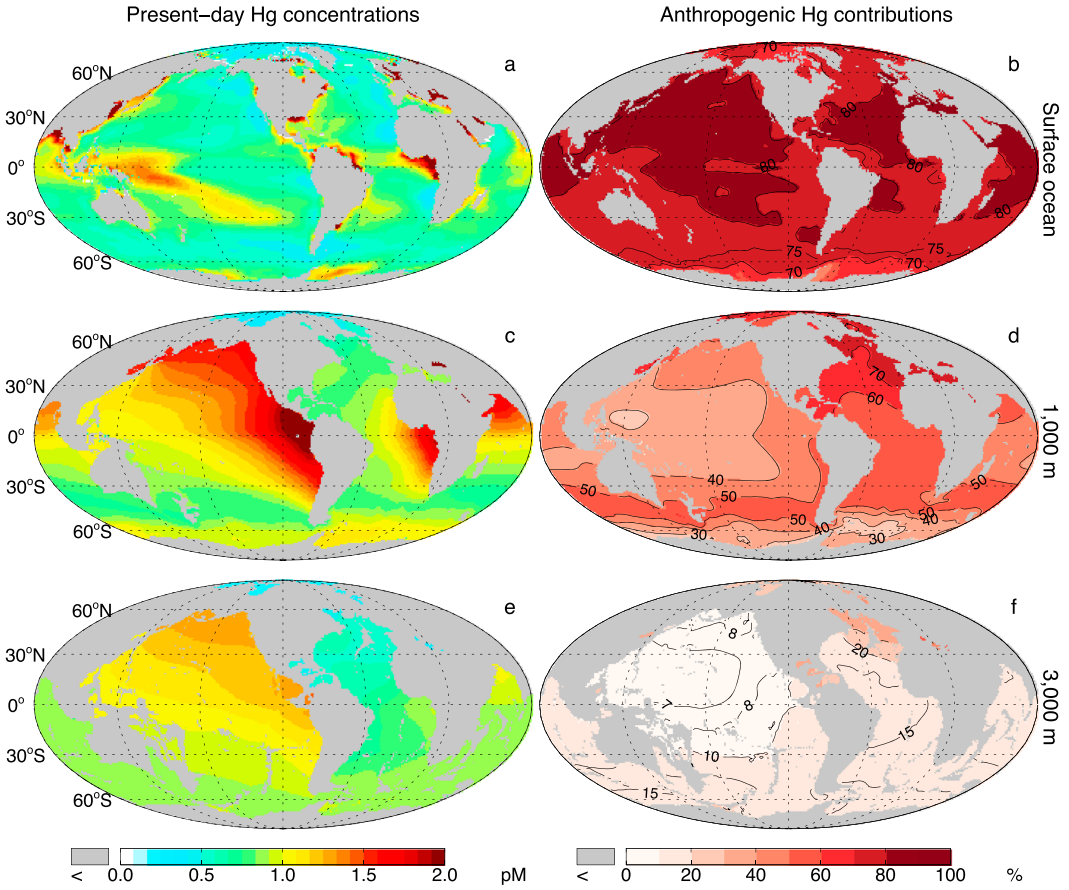

Figure 3. Spatial distribution of Hg concentrations in the present-day ocean. Annual mean concentrations of total Hg (in pM) for (a) the mixed layer, (c) 1000 m depth, and (e) 3000 m depth. (b, d, and f) Contributions of anthropogenic Hg to the present-day concentrations, expressed in percentage.

upwelling such as the Weddell Sea. The modeled total Hg concentrations increase with depth, from 0.72 pM in the mixed layer to 1 pM at 3000 m (Figure 3e). This reflects removal of Hg from the surface to the subsurface ocean by particle sinking followed by remineralization at depth [*Zhang et al.*, 2014; *Lamborg et al.*, 2014b].

At 3000 m depth, modeled Hg concentrations predict progressive enrichment with length of time since the water was in contact with the surface: the lowest Hg concentrations (~0.5 pM) are in the young waters of the North Atlantic Ocean, increasing to 1 pM in the South Pacific and Indian Oceans and reaching up to 1.4 pM in the North Pacific Ocean (Figure 3e). The continuous input of Hg from particle remineralization as the water transits from the North Atlantic to the North Pacific leads to a factor of 3 increase in Hg concentrations. At 1000 m depth, Hg concentrations show similar interbasin differences as at 3000 m (Figure 3c). Concentrations reaching up to 1.8–2 pM are predicted in the eastern equatorial Atlantic and Pacific Oceans, due to high input from sinking organic particles. These two regions are also characterized by low oxygen concentrations. In general, the distribution of Hg and oxygen tend to be anticorrelated: as organic material degrades in deep water, oxygen is consumed and Hg is released [*Zhang et al.*, 2014]. Modeled vertical profiles predict that high Hg concentrations in the North Pacific Ocean extend to 500–1500 m depth poleward of 40°N (Figure 4b). High concentrations are also modeled throughout the tropics in both the Atlantic and Pacific basins at depths of 500–1000 m. Upwelling and downwellling processes associated with upper layer divergence and convergence also modify Hg distributions in the upper 1000 m.

Over the subarctic North Atlantic Ocean, observations of Hg concentration profiles suggest fairly uniform concentrations with depth (Figure 4c), reflecting deep water formation and rapid vertical mixing [*Schmittner et al.*, 2007]. In other regions, most of the observed Hg concentration profiles have subsurface peaks at

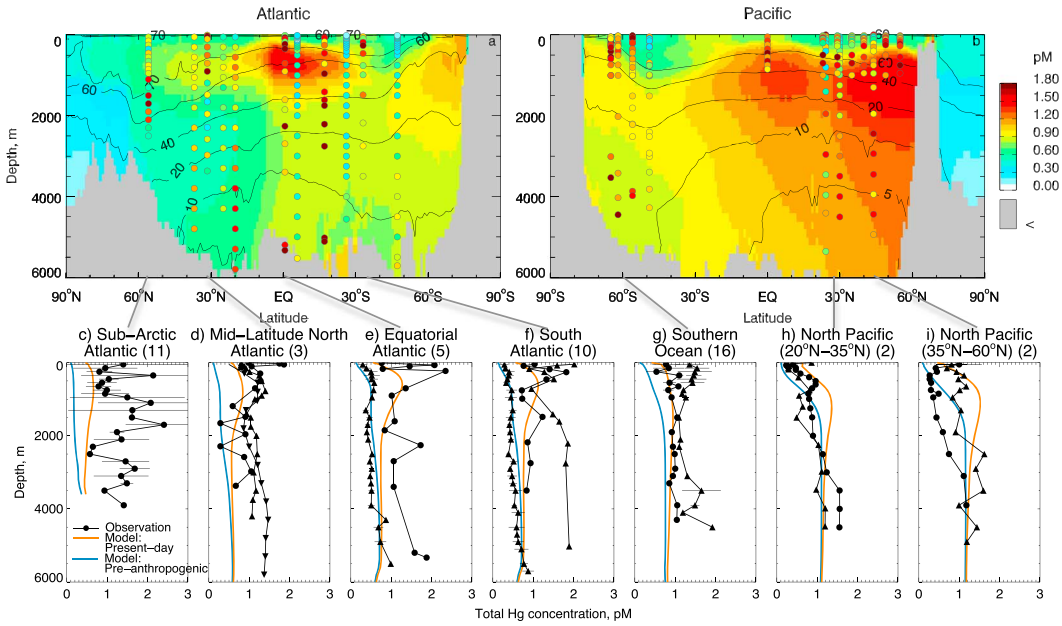

Figure 4. Vertical distribution of oceanic Hg. Zonal mean cross sections of total Hg concentrations (filled contours, in pM) for the (a) Atlantic Ocean and (b) Pacific Ocean. The black contours indicate the percent contribution from anthropogenic Hg. The bottom panels display observed total Hg concentration profiles (black symbols, see Table 1) for the (c) subarctic Atlantic, (d) midlatitude North Atlantic, (e) equatorial Atlantic, (f) South Atlantic, (g) Southern Ocean, (h) North Pacific (20°N–35°N), and (i) North Pacific (35°N–60°N). The number of observed profiles used in the comparison is indicated in parenthesis for each panel. The solid lines indicate modeled profiles for the preanthropogenic (blue) and present-day (orange) simulation.

500–800 m depth (Figures 4d, 4e, 4f, 4h, and 4i). On average, the model reproduces the observed total Hg concentrations at 0–100 m (model: 0.69 ± 0.27 pM; obs: 0.78 ± 0.58 pM), 100–1000 m (model: 0.94 ± 0.27 pM, obs: 1.0 ± 0.97 pM), and >1000 m (model: 0.88 ± 0.21 pM; obs: 0.83 ± 0.60 pM). Despite the large variability within each profile and among profiles in the same region (Figures 4e, 4f, and 4i), the model generally reproduces the vertical structure. Overall, the model is within 50% of the observed Hg profiles, with the exception of measurements in the high and midlatitude North Atlantic Ocean (Figures 4c and 4d).

The model captures the shallower portion (<1500 m) of the observed profiles over the subarctic and midlatitude North Atlantic Ocean (Figures 4c and 4d) but is too low by a factor of 2 below those depths. Long-term observations near Bermuda indicate that the North Atlantic Hg concentrations in the top 1000 m were 5 to 10 times higher in the 1980s and 1990s compared to today [*Soerensen et al.*, 2012, and references therein]. This trend could partially be caused by widespread commercial use of Hg in the U.S. and Europe, and its unregulated release until the late 1980s [*Horowitz et al.,* 2014]. The resulting high Hg riverine runoff and wastewater discharge to the Atlantic Ocean could contribute to the elevated Hg concentrations observed in the North Atlantic [*Amos et al.*, 2014]. These releases of commercial Hg are not included in our simulation. Assuming that the difference between observations and modeled profiles below 1500 m in the North Atlantic is due to this missing commercial Hg source, the model discrepancy suggests that the missing source could account for an additional 40 Mmol of anthropogenic Hg in the ocean.

3.3. Penetration of Anthropogenic Hg in the Oceans

We calculate the anthropogenic contribution to present-day Hg concentrations by differencing the present-day simulation (year 2008) and our preanthropogenic simulation. In surface waters, we find that 77% of the Hg is anthropogenic in origin (Figure 3b). The distribution of the anthropogenic contribution is relatively uniform in the surface ocean, with slightly lower contributions in polar regions, which are shielded from atmospheric deposition by sea ice. At 1000 m depth, the anthropogenic contribution is not as evenly distributed, with the largest contributions (>70%) occurring over the North Atlantic Ocean where North Atlantic Deep Water is formed. This is then advected into the interior (Figure 3d). A secondary maximum at

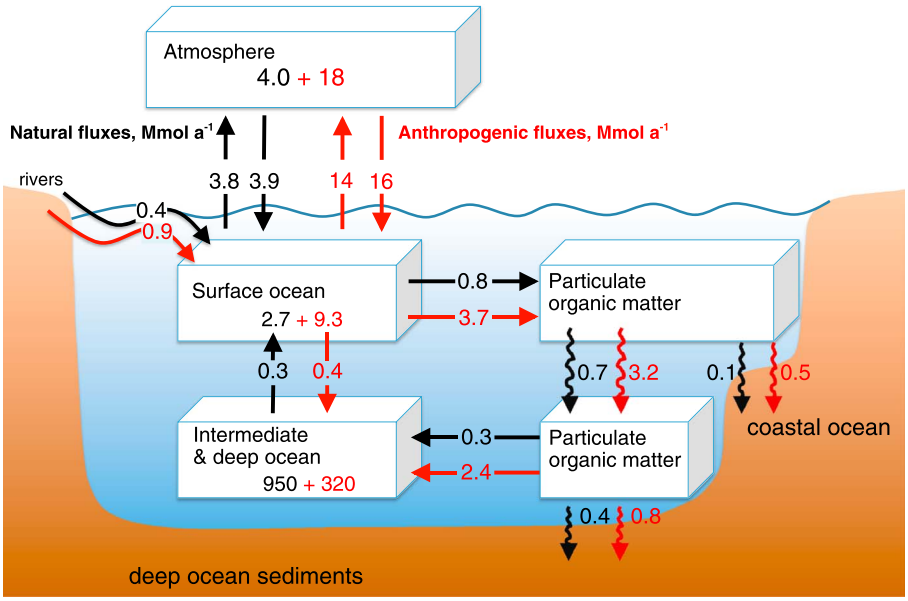

Figure 5. Human influence on the marine Hg cycle. The numbers in the boxes correspond to the mass of Hg in each reservoir (in units of Mmol), while the arrows indicate fluxes in Mmol a^{-1}. The preanthropogenic conditions are in black arrows and numbers, while the human perturbation is shown in red.

1000 m occurs in the Southern Ocean between 30 and 50°S, where Antarctic Intermediate Water are found. The anthropogenic contribution decreases to 10–20% at 3000 m depth and <10% below 4,000 m (Figures 3f, 4a, and 4b).

A comparison of Hg concentration profiles in the present-day ocean simulation to the model preanthropogenic profiles allows us to investigate the distribution of anthropogenic Hg concentrations in the ocean (Figures 4c–4j). Over the subarctic North Atlantic (Figure 4c) and Southern Ocean (Figure 4g) efficient vertical transport leads to uniform anthropogenic Hg concentrations down to 3000 m. Elsewhere, the modeled anthropogenic Hg concentrations reach peak concentrations of 0.5–0.8 pM at 400–500 m, where sinking particles remineralize. We thus predict that the observed subsurface maxima in Hg concentrations in these ocean basins are associated with the accumulation of anthropogenic Hg (Figures 4d, 4e, 4f, and 4h). Below 2000 m depth, the anthropogenic Hg concentrations are low (0.1–0.2 pM) because this water has been sequestered from the surface for hundreds of years.

The model simulation allows quantification of the anthropogenic perturbation to the present-day mercury marine cycle (Figure 5). Our ocean Hg model suggests that anthropogenic Hg enters the ocean via atmospheric deposition at a rate of 16 Mmol a^{-1}, with another 0.9 Mmol a^{-1} from rivers. These fluxes are the result of both direct Hg anthropogenic emissions and recycling of legacy emissions. Air-sea exchange leads to the net evasion of 14 Mmol a^{-1} back to the atmosphere. Anthropogenic Hg penetrates into the ocean interior via two mechanisms: physical transport away from deep and intermediate/mode water formation regions (the physical pump) and remineralization of sinking organic particles (often referred to as the biological pump). Our model suggests that the physical pump accounts for the transport of 0.4 Mmol a^{-1} and that the biological pump is the dominant pathway for anthropogenic Hg penetration, with a flux of 3.7 Mmol a^{-1}. About 15% of the

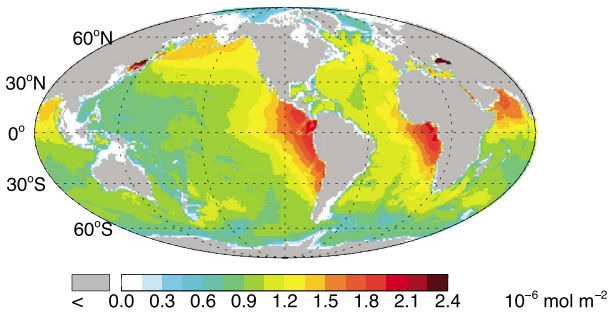

Figure 6. Column inventory of anthropogenic Hg in the ocean. Anthropogenic Hg concentrations are vertically integrated and displayed in units of 10^{-6} mol m^{-2}.

sinking particles undergo sedimentation in coastal areas and the rest reach intermediate and deep ocean regions. Once in deeper ocean waters, 71% of the anthropogenic Hg attached to sinking organic particles is remineralized back to dissolved Hg, with the remaining 29% undergoing sedimentation to the deep ocean floor.

The modeled column inventory of anthropogenic Hg in the ocean shows the role of the biological pump in controlling the distribution of anthropogenic Hg in the oceans (Figure 6). The model predicts elevated anthropogenic Hg in three regions with active productivity and particle sinking: the eastern tropical Atlantic Ocean and Pacific Oceans and the Arabian Sea. Together, these three regions account for 17% of the total anthropogenic burden, but only 10% of the ocean surface. Smaller enhancements are predicted in the high-latitude North Pacific Oceans. Advection by the physical pump generates a smaller increase in anthropogenic Hg column concentrations in the Atlantic Ocean. The lowest values are for the Arctic Ocean and coastal and near-shelf regions, because of the shallow depth.

It is interesting to draw parallels between anthropogenic CO_2 and anthropogenic Hg in the ocean as both have similar emissions history, wide dispersal in the atmosphere, and vigorous air-sea exchange [*Lamborg et al.*, 2014a]. The ocean sink accounts for 30% of the 555 PgC anthropogenic CO_2 emitted to the atmosphere since 1750 [*Ciais et al.*, 2013]. For Hg, we find that the ocean has stored 35% of anthropogenic emissions since 1450, with an additional 15% in ocean sediments. Thus, in both cases the ocean plays a central role in controlling the fate of anthropogenic emissions. However, the penetration pathways, and resulting oceanic distribution of anthropogenic Hg and carbon, are very different. Anthropogenic CO_2 invades the ocean via gas exchange and is transported into the ocean interior by advection/diffusion (i.e., solubility pump). Indeed, as inorganic carbon is generally not a limiting factor for oceanic primary production [*Raven and Johnston*, 1991], the transport of carbon to the deep ocean via the biological pump remains nearly unchanged over the anthropocene [*Denman et al.*, 2007]. Observational and model-based estimates show that the highest inventories of anthropogenic CO_2 in the oceans are associated with deep water formation in the North Atlantic and intermediate/mode water formation in the Southern Ocean [*Sabine et al.*, 2004; *Waugh et al.*, 2006]. In contrast, anthropogenic Hg enters the ocean via atmospheric deposition and is carried downward predominantly through the biological pump (Figure 6). This leads to most of the anthropogenic Hg residing in subsurface waters of biological productive regions (Figure 5) and penetrating to deeper depths compared to anthropogenic CO_2. Indeed, *Sabine et al.* [2004] found that about 30% of the anthropogenic CO_2 is located at depths shallower than 200 m, and nearly half at depths above 400 m. For anthropogenic Hg our model predicts that 80% of the anthropogenic marine Hg resides at depths deeper than 400 m. Therefore, using anthropogenic CO_2 as a proxy, *Lamborg et al.* [2014a] may have underestimated the fraction of anthropogenic Hg in the deep ocean. Indeed, they find that 100 Mmol is in the deep ocean, while we calculate nearly 50% more (148 Mmol).

Unlike inorganic carbon measurements in the ocean, Hg measurements are very sparse, and thus, our calculation of the anthropogenic Hg inventory in the oceans is poorly constrained by observations. Our estimate of 330 Mmol anthropogenic Hg in the oceans has large uncertainties associated with historical emissions of Hg as well as with our assumptions for key parameters in oceanic Hg biochemistry and potential model biases. We estimate that these factors lead to a range of 190–530 Mmol anthropogenic Hg in the oceans (see supporting information). More systematic global measurements of speciated Hg concentrations in the world's oceans, as part of the ongoing GEOTRACES (www.geotraces.org) and Climate Variability and Predictability (CLIVAR) (http://www.clivar.org) programs, will provide better observational constraints on the storage of anthropogenic Hg in the oceans. In particular, targeting regions where we predict elevated concentrations of anthropogenic Hg (eastern equatorial Atlantic, eastern equatorial Pacific, Indian, and high-latitude North Pacific) will help elucidate the connection between the biological pump and anthropogenic Hg.

Acknowledgments

Y.Z. thanks H. Amos for providing box model results, D. Trossman and A. Shao for helping with OFFTRAC model development, and S. Emerson for helpful discussions. We acknowledge all the scientists who have participated in the collection and analysis of the oceanic and lake sediment observations used in this study. All the data sets used in this paper are available upon request (Y.Z. yxzhang@seas.harvard.edu).

References

Amos, H. M., et al. (2012), Gas-particle partitioning of atmospheric Hg(II) and its effect on global mercury deposition, *Atmos. Chem. Phys.*, *12*, 591–603.

Amos, H. M., D. J. Jacob, D. G. Streets, and E. M. Sunderland (2013), Legacy of all-time anthropogenic emissions on the global mercury cycle, *Global Biogeochem. Cycles*, *27*, 410–421, doi:10.1002/gbc.20040.

Amos, H. M., D. J. Jacob, D. Kocman, H. M. Horowitz, Y. Zhang, S. Dutkiewicz, M. Horvat, E. S. Corbitt, D. P. Krabbenhoft, and E. M. Sunderland (2014), Global biogeochemical implications of mercury discharges from rivers and sediment burial, *Environ. Sci. Technol.*, doi:10.1021/es502134t.

Bowman, K. L., T. Kading, G. J. Swarr, C. H. Lamborg, C. R. Hammerschmidt, and M. Rijkenberg (2012), Mercury species and thiols from GEOTRACES cruises in the North and South Atlantic Ocean, in Goldschmidt Conference, Montreal, Canada.

Bowman, K. L., C. R. Hammerschmidt, C. H. Lamborg, and G. Swarr (2014), Mercury in the North Atlantic Ocean: The U.S. GEOTRACES zonal and meridional transects, *Deep Sea Res., Part II*, doi:10.1016/j.dsr2.2014.07.004.

Ciais, P., et al. (2013), Carbon and other biogeochemical cycles, in *Climate Change 2013: The Physical Science Basis. Contribution of Working Group I to the Fifth Assessment Report of the Intergovernmental Panel on Climate Change*, edited by T. F. Stocker et al., Cambridge Univ. Press, Cambridge, U. K., and New York.

Cooke, C. A., P. H. Balcom, H. Biester, and A. P. Wolfe (2009), Over three millennia of mercury pollution in the Peruvian Andes, *Proc. Natl. Acad. Sci. U.S.A.*, *106*(22), 8830–8834.

Cossa, D., L.-E. Heimbürger, D. Lannuzel, S. R. Rintoul, E. C. V. Butler, A. R. Bowie, B. Averty, R. J. Watson, and T. Remenyi (2011), Mercury in the Southern Ocean, *Geochim. Cosmochim. Acta*, *75*(14), 4037–4052.

Dai, A., and K. E. Trenberth (2002), Estimates of freshwater discharge from continents: Latitudinal and seasonal variations, *J. Hydrometeorol.*, *3*, 660–687.

Denman, K. L., et al. (2007), Couplings between changes in the climate system and biogeochemistry, in *Climate Change 2007: The Physical Science Basis. Contribution of Working Group I to the Fourth Assessment Report of the Intergovernmental Panel on Climate Change*, edited by S. Solomon et al., Cambridge Univ. Press, Cambridge, U. K., and New York.

Dunne, J. P., R. A. Armstrong, A. Gnanadesikan, and J. L. Sarmiento (2005), Empirical and mechanistic models for the particle export ratio, *Global Biogeochem. Cycles*, *19*, GB4026, doi:10.1029/2004GB002390.

Ebinghaus R., C. Banic, S. Beauchamp, D. Jaffe, H. H. Kock, N. Pirrone, L. Poissant, F. Sprovieri, and P. S. Weiss-Penzias (2009), Spatial coverage and temporal trends of land-based atmospheric mercury measurement in the Northern and Southern Hemispheres, in *Mercury Fate and Transport in the Global Atmosphere*, edited by N. Pirrone and R. P. Mason, chap. 9, Springer.

Elbaz-Poulichet, F., L. Dezileau, R. Freydier, D. Cossa, and P. Sabatier (2011), A 3500-year record of Hg and Pb contamination in a Mediterranean sedimentary archive (the Pierre Blanche Lagoon, France), *Environ. Sci. Technol.*, *45*(20), 8642–8647.

Engstrom, D. R., W. F. Fitzgerald, C. A. Cooke, C. H. Lamborg, P. E. Drevnick, E. B. Swain, S. J. Balogh, and P. H. Balcom (2014), Atmospheric Hg emissions from preindustrial gold and silver extraction in the Americas: A reevaluation from lake-sediment archives, *Environ. Sci. Technol.*, *48*, 6533–6543.

Fitzgerald, W. F., D. R. Engstrom, C. H. Lamborg, C. M. Tseng, P. H. Balcom, and C. R. Hammerschmidt (2005), Modern and historic atmospheric mercury fluxes in northern Alaska: Global sources and Arctic depletion, *Environ. Sci. Technol.*, *39*, 557–568.

Fitzgerald, W. F., C. H. Lamborg, and C. R. Hammerschmidt (2007), Marine biogeochemical cycling of mercury, *Chem. Rev.*, *107*, 641–662.

Guerrero, S. (2012), Chemistry as a tool for historical research: Identifying paths of historical mercury pollution in the Hispanic New World, *Bull. Hist. Chem.*, *37*, 61−70.

Hallberg, R., and P. Rhines (1996), Buoyancy-driven circulation in an ocean basin with isopycnals intersecting the sloping boundary, *J. Phys. Oceanogr.*, *26*, 913–940.

Hammerschmidt, C. R., and K. L. Bowman (2012), Vertical methylmercury distribution in the subtropical North Pacific Ocean, *Mar. Chem.*, *132–133*, 77–82.

Holmes, C. D., D. J. Jacob, E. S. Corbitt, J. Mao, X. Yang, R. Talbot, and F. Slemr (2010), Global atmospheric model for mercury including oxidation by bromine atoms, *Atmos. Chem. Phys.*, *10*(24), 12,037–12,057.

Horowitz, H. M., D. J. Jacob, H. M. Amos, D. G. Streets, and E. M. Sunderland (2014), Historical mercury releases from commercial products: Global environmental implications, *Environ. Sci. Technol.*, *48*(17), 10,242–10,250.

Joos, F., M. Bruno, R. Fink, U. Siegenthaler, T. F. Stocker, C. Le Quéré, and J. Sarmiento (1996), An efficient and accurate representation of complex oceanic and biospheric models of anthropogenic carbon intake, *Tellus B*, *48*(3), 397–417.

Kalnay, E., et al. (1996), The NCEP/NCAR 40-year reanalysis project, *Bull. Am. Meteorol. Soc.*, *77*, 437–470.

Lacerda, L. D. (1997), Global mercury emissions from gold and silver mining, *Water Air Soil Pollut.*, *97*, 209–221.

Ladd, C., and L. Thompson (2001), Water mass formation in an isopycnal model of the North Pacific, *J. Phys. Oceanogr.*, *31*, 1517–1537.

Lamborg, C. H., W. F. Fitzgerald, J. O'Donnel, and T. Torgersen (2002), A non-steady-state compartmental model of global-scale mercury biogeochemistry with interhemispheric atmospheric gradients, *Geochem. Cosmochim. Acta*, *66*, 1105–1118.

Lamborg, C. H., C. R. Hammerschmidt, G. A. Gill, R. P. Mason, and S. Gichuki (2012), An intercomparison of procedures for the determination of total mercury in seawater and recommendations regarding mercury speciation during GEOTRACES cruises, *Limnol. Oceanogr. Method*, *10*, 90–100.

Lamborg, C. H., C. R. Hammerschmidt, K. L. Bowman, G. J. Swarr, K. M. Munson, D. C. Ohnemus, P. J. Lam, L.-E. Heimbürger, M. J. A. Rijkenberg, and M. A. Saito (2014a), Anthropogenic mercury in the ocean estimated from water column measurements, *Nature*, *512*, 65–68.

Lamborg, C., K. Bowman, C. Hammerschmidt, C. Gilmour, K. Munson, N. Selin, and C.-M. Tseng (2014b), Mercury in the anthropocene ocean, *Oceanography*, *27*(1), 76–87.

Large, W. G., and S. G. Yeager (2009), The global climatology of an interannually varying air-sea flux data set, *Clim. Dyn.*, *33*(2–3), 341–364.

Laurier, F. J. G., R. P. Mason, G. A. Gill, and L. Whalin (2004), Mercury distributions in the North Pacific Ocean—20 years of observations, *Mar. Chem.*, *90*, 3–19.

Mason, R. P., and W. F. Fitzgerald (1993), The distribution and biogeochemical cycling of mercury in the equatorial pacific-ocean, *Deep Sea Res., Part I*, *40*(9), 1897–1924.

Mason, R. P., and G. R. Sheu (2002), Role of the ocean in the global mercury cycle, *Global Biogeochem. Cycles*, *16*(4), 1093, doi:10.1029/2001GB001440.

Mason, R. P., and K. A. Sullivan (1999), The distribution and speciation of mercury in the South and equatorial Atlantic, *Deep Sea Res., Part II*, *46*, 937–956.

Mason, R. P., W. F. Fitzgerald, and F. M. M. Morel (1994), The biogeochemical cycling of elemental mercury: Anthropogenic influences, *Geochem. Cosmochim. Acta*, *58*, 3191–3198.

Mason, R. P., K. R. Rolfhus, and W. F. Fitzgerald (1998), Mercury in the North Atlantic, *Mar. Chem.*, *61*(1–2), 37–53.

Mason, R. P., N. M. Lawson, and G. R. Sheu (2001), Mercury in the Atlantic Ocean: Factors controlling air-sea exchange of mercury and its distribution in the upper waters, *Deep Sea Res., Part II*, *48*, 2829–2853.

Mason, R. P., A. L. Choi, W. F. Fitzgerald, C. R. Hammerschmidt, C. H. Lamborg, A. L. Soerensen, and E. M. Sunderland (2012), Mercury biogeochemical cycling in the ocean and policy implications, *Environ. Res.*, *119*, 101–117.

Morel, F. M. M., A. M. L. Kraepiel, and M. Amyot (1998), The chemical cycle and bioaccumulation of mercury, *Annu. Rev. Ecol. Syst.*, *29*, 543–566.

Nriagu, J. O. (1993), Legacy of mercury pollution, *Nature*, *363*, 589.

Pacyna, E. G., J. M. Pacyna, K. Sundseth, J. Munthe, K. Kindbom, S. Wilson, F. Steenhuisen, and P. Maxson (2010), Global emission of mercury to the atmosphere from anthropogenic sources in 2005 and projections to 2020, *Atmos. Environ.*, *44*, 2487–2499.

Raven, J. A., and A. M. Johnston (1991), Mechanisms of inorganic-carbon acquisition in marine phytoplankton and their implications for the use of other resources, *Limnol. Oceanogr.*, *36*(8), 1701–1714.
Sabine, C. L., et al. (2004), The oceanic sink for anthropogenic CO_2, *Science*, *305*, 367–371.
Schmittner, A., J. C. H. Chiang, and S. R. Hemming (2007), Introduction: The ocean's meridional overturning circulation, *Geophys. Monogr. Ser.*, *173*, doi:10.1029/173GM02.
Selin, N. E., D. J. Jacob, R. J. Park, R. M. Yantosca, S. Strode, L. Jaegle, and D. Jaffe (2007), Chemical cycling and deposition of atmospheric mercury: Global constraints from observations, *J. Geophys. Res.*, *112*, D02308, doi:10.1029/2006JD007450.
Selin, N. E., D. J. Jacob, R. M. Yantosca, S. Strode, L. Jaegle, and E. M. Sunderland (2008), Global 3-D land-ocean atmosphere model for mercury: Present-day versus preindustrial cycles and anthropogenic enrichment factors for deposition, *Global Biogeochem. Cycles*, *22*, GB2011, doi:10.1029/2007GB003040.
Siegenthaler, U., and H. Oeschger (1978), Predicting future atmospheric carbon dioxide levels, *Science*, *199*(4327), 388–395.
Soerensen, A. L., E. M. Sunderland, C. D. Holmes, D. J. Jacob, R. M. Yantosca, H. Skov, J. H. Christensen, S. A. Strode, and R. P. Mason (2010), An improved global model for air-sea exchange of mercury: High concentrations over the North Atlantic, *Environ. Sci. Technol.*, *44*(22), 8574–8580.
Soerensen, A. L., D. J. Jacob, D. G. Streets, M. L. I. Witt, R. Ebinghaus, R. P. Mason, M. Andersson, and E. M. Sunderland (2012), Multi-decadal decline of mercury in the North Atlantic atmosphere explained by changing subsurface seawater concentrations, *Geophys. Res. Lett.*, *39*, L21810, doi:10.1029/2012GL053736.
Sprovieri, F., N. Pirrone, R. Ebinghaus, H. Kock, and A. Dommergue (2010), A review of worldwide atmospheric mercury measurements, *Atmos. Chem. Phys.*, *10*, 8245−8265.
Streets, D. G., M. K. Devane, Z. Lu, T. C. Bond, E. M. Sunderland, and D. J. Jacob (2011), All-time releases of mercury to the atmosphere from human activities, *Environ. Sci. Technol.*, *45*, 10,485–10,491.
Strode, S., L. Jaeglé, and N. E. Selin (2009), Impact of mercury emissions from historic gold and silver mining: Global modeling, *Atmos. Environ.*, *43*, 2012–2017.
Strode, S., L. Jaeglé, and S. Emerson (2010), Vertical transport of anthropogenic mercury in the ocean, *Global Biogeochem. Cycles*, *24*, GB4014, doi:10.1029/2009GB003728.
Strode, S. A., L. Jaeglé, N. E. Selin, D. J. Jacob, R. J. Park, R. M. Yantosca, R. P. Mason, and F. Slemr (2007), Air-sea exchange in the global mercury cycle, *Global Biogeochem. Cycles*, *21*, GB1017, doi:10.1029/2006GB002766.
Sunderland, E., and R. Mason (2007), Human impacts on open ocean mercury concentrations, *Global Biogeochem. Cycles*, *21*, GB4022, doi:10.1029/2006GB002876.
Sunderland, E. M., D. P. Krabbenhoft, J. W. Moreau, S. A. Strode, and W. M. Landing (2009), Mercury sources, distribution, and bioavailability in the North Pacific Ocean: Insights from data and models, *Global Biogeochem. Cycles*, *23*, GB2010, doi:10.1029/2008GB003425.
Waugh, D. W., T. M. Hall, and B. I. McNeil (2006), Anthropogenic CO_2 in the oceans estimated using transit-time distributions, *Tellus*, *58*, 376–389.
Zhang, Y., et al. (2012), Nested-grid simulation of mercury over North America, *Atmos. Chem. Phys.*, *12*, 6095–6111.
Zhang, Y., L. Jaeglé, and L. Thompson (2014), Natural biogeochemical cycle of mercury in a global three-dimensional ocean tracer model, *Global Biogeochem. Cycles*, *28*, 553–570, doi:10.1002/2014GB004814.